Transformation of plant biomass waste into resourceful activated carbon nanostructures for mixed-assembly type electrochemical capacitors

Damilola Momodu[1], Chiamaka Okafor[2], Ncholu Manyala[1]*, Abdulhakeem Bello[1,2], Martiale Gaetan ZebazeKana[2,3] and Esidor Ntsoenzok [2,4].

[1]Department of Physics, Institute of Applied Materials, SARCHI Chair in Carbon Technology and Materials, University of Pretoria, Pretoria 0028, South Africa.

[2]Department of Materials Science and Engineering, African University of Science and Technology, Federal Capital Territory, Abuja, Nigeria

[3]Department of Materials Science and Engineering, Kwara State University, Malete, Nigeria.

[4] Department of Physics CEHMTI – Centre National de la Recherche Scientifique, Orleans, France.

*Corresponding author's email: Ncholu.Manyala@up.ac.za.

ABSTRACT

Activated carbon (AC) was obtained from three different plant biomass wastes sources (coconut shell, pine cones and rice husk) via hydrothermal treatment followed by carbonization at 800 °C for different times. The morphological and structural characteristics of the transformed carbon material revealed a highly disordered graphitic carbon composed of a porous network with energy storage capability. The mixed-assembly type cells fabricated from the best samples based on specific capacitance from the single electrode tests exhibited electric double layer capacitance (EDLC) behaviour in all sample combinations using all the three transformed activated carbon materials. The mixed-assembly device worked comfortably in a voltage window of 1.5 V in neutral aqueous electrolyte. A specific capacitance (C_S) of ~110 F g^{-1} was obtained with a corresponding energy density of 8.5 W h kg^{-1} and power density of 380 W kg^{-1} at a current density of 0.5 A g^{-1} for the PC_RH device An excellent stability was exhibited with a coulombic efficiency of a 99.7% and capacitance retention of 80% after 10000 continuous cycling at 5.0 A g^{-1}. Furthermore, subjecting the PC_RH mixed device to a floating test for ~48 h (2 days) at its optimum voltage (1.5 V) revealed retention in the capacitance value to more than 50% its initial value with still no recorded device failure. Remarkably, the asymmetric design showed a potential for adopting EDLC materials of different carbon sources in order to capture the entire properties for efficient and stable energy storage devices.

Keywords: Plant waste; Energy storage materials; Activated carbon; Mixed-assembly; Supercapacitors

1. INTRODUCTION

As the global economy constantly continues to rise, the global demand for power and energy sources are synonymously increasing. This raises the consumption of fossil fuels which produces two major related issues; depletion of fossil fuel reserves and environmental green-house gas emission problem which not only pose pollution problems but also climate change concerns. These matters have been projected as one of the urgent challenges to be tackled. Therefore, there is a need to develop clean and sustainable alternative energy sources that meet up with the rising global energy demand. In view of this, a lot of renewable energy sources have been explored; but they generally have a common related issue; i.e. they are seasonal. Most renewable clean energy sources are highly dependent on the time of day and regional weather conditions. The need for the development of related energy conversion and storage devices therefore arises in order to harness these renewable clean energy [1]. Energy conversion and storage devices which show great potential currently include fuel cells, batteries, and supercapacitors.

Supercapacitors, (SCs) store energy physically as charge and are seen to be the bridge between normal parallel plate capacitors and batteries [2]. They are known to have higher power densities, longer cycling stability and, operate at wider temperature range as compared to batteries. Although they are plagued with lower energy densities when compared with batteries, extensive research has been devoted to overcoming this challenge. SCs can be broadly divided into three (3) types in relation to their principle of charge storage namely; electric double layer capacitors (EDLCs), Pseudocapacitors/Redox Electrochemical capacitors (PCs/RECs) and Hybrid supercapacitors (hySCs). EDLCs work solely by the separation of electrostatic charge at the electrode/electrolyte interface while RECs depend on fast redox processes involving the transfer of charges between the electrode/electrolyte

interfaces [3, 4]. The hySCs are usually composed of a combination of both storage mechanism properties of the EDLC and RECs.

EDLCs are mainly based on carbonaceous materials and operates based on pure charge separation. They have been widely developed industrially due to its cost effectiveness based on abundance of carbon materials, long cyclic stability, fast charge-discharge kinetics, low maintenance costs and larger energy density etc when compared to the other types of SCs such as electrolytic capacitors [5–8]. However, the nature of the electrolytes used at the commercial scale still impedes their extensive application. The discovery of cheaper and reliable materials along with an effective environmentally stable/safe electrolyte for equally enhanced performance EDLC devices will greatly steer the energy storage research in a new direction.

The use of biomass waste materials is seen to be a new dimension in this regard due to their abundance as low-value materials which sometimes pose an environmental threat (in terms of pollution) to social life and risk to health when not properly disposed as thrash. Thus, a possibility to convert these materials from trash to treasure paves way to save cost as well as sanitize our environment [9, 10]. The as-prepared carbonaceous sample are characterized with fine-tuned properties suitable for specific applications. For example, highly porous hierarchical activated carbon nanostructures are widely adopted as electrode materials for energy storage and are known to have high surface area, necessary pore size distribution, good electrical conductivity, thermal stability, chemical stability amongst others [11, 12].

Numerous researchers have extensively carried out studies on various biomass waste materials for different applications including supercapacitor materials by adopting physical and chemical activation processes [13–22]. For example, rice husk was converted into activated carbon (AC) using $ZnCl_2$ as activating agent [17]. The obtained product possessed a

high specific surface area (SSA) of 1442 m^2 g^{-1} with an energy density of up to 8.36 Wh kg^{-1} and good capacitance retention after 1000 cycles. In another report in [19], activated carbon from pine cones was synthesized by initial hydrothermal treatment to increase the amount of carbon-content in the raw material before KOH-activation and carbonization at 800 °C. The AC material adopted as a supercapacitor material exhibited a high SSA value of 1515 m^2 g^{-1} and a corresponding specific capacitance of 137 F g^{-1} in a neutral electrolyte. The use of a neutral electrolyte is linked to the ease of handling coupled with their relatively large operating voltages linked to their pH, strong ion solvation and high over potential for di-hydrogen evolution [19, 23, 24]. R. Farma et *al*. [20] synthesized highly porous activated carbon electrodes from oil palm bunches by N_2-carbonization and CO_2-activation, the device exhibited a specific capacitance (C_s) of 150 F g^{-1}, energy density of 4.297 Wh kg^{-1} and a power density of 173 W kg^{-1}. Although most of these reports have adopted different carbon-containing biomass precursors to assemble supercapacitor devices, the present study embarks on a transformation of biomass waste from three different plant materials (coconut shell, pine cone and rice husk) into highly porous activated carbon. Furthermore, coupling of dissimilar carbon-based electrodes in form of an asymmetric or mixed device assembly is done to analyze their electrochemical performance. The reason behind putting these different materials from the various biomass sources together is to maximally amass their individual storage features in one EDLC device.

Material analysis confirmed the presence of a three dimensional interconnected pore network suitable for active ion transport and storage. These results obtained depict the potential of adopting such device configurations with neutral aqueous electrolytes for the design of relatively cheaper, efficient and stable SC devices.

2. MATERIALS SYNTHESIS AND CHARACTERIZATION METHODS

All chemicals were of research grade, high purity and were used as received without additional purification. The biomass waste raw materials (coconut shells, pine cones, rice husks) were obtained from fruit vendors, open fields and nearby rice farms.

2.1. Synthesis of Activated Carbon from waste materials

The raw waste materials (coconut shells, rice husk) were obtained from a local farm while the pine cones were picked from the green park area around the African University of Science and Technology (AUST) campus in Galadimawa, Nigeria. The raw materials were then washed with distilled water and acetone (50:50 wt. vol) to remove any impurities such as adhered dirt or processing dirt from handling or transportation before drying in an oven at 80 °C temperature. Initial processing of the raw material was carried out by crushing of the coconut shell, pine cones and rice husks into smaller fragments of about 0.5 cm dimensions. Subsequently, a known mass of each raw material (5.0 g) was mixed with a 100 ml solution containing 0.5 ml of 1 M sulphuric acid and water to ensure the removal of cellulose present in the plant biomass waste and possible increase of carbon content. The mixture was then subjected to hydrothermal treatment in a locally modified autoclave system at 180 °C for 6 h. The solid black product was then washed thoroughly with distilled water and dried at 80 °C. Chemical activation with KOH was carried out on all samples in a 1:1 mass ratio for the KOH to active raw material respectively. Carbonization was done on all the autoclaved samples at 800 °C (at 20 °C min^{-1} ramp rate) in a quartz tubular furnace for different carbonization times (i.e. 1 h, 2 h & 3 h) under argon gas flow at 10 cm^3 min^{-1}. The final products were left to cool down naturally to room temperature under argon flow to avoid excess oxidation of the samples and proper pore evolution. Further washing was carried out on the final carbonized

samples with 1 M HCl to remove any unreacted KOH and distilled water to obtain a neutral powder sample. These samples were then labelled as AC-M-N where M denotes the material precursor and N denotes the carbonization time in hours.

Proximate and Yield analysis were performed on the biomass derived activated carbons with the best charge storage ability based on the calculated specific capacitance to ascertain the moisture content, ash content, volatile matter, fixed carbon content and material yield. To do this, a known mass of the powder sample was subjected to heating at different temperatures in both vacuum and air to obtain the moisture content (MC), ash content (AsC) and volatile matter (VM) content. In order to determine the moisture content, 1 g of each of the sample product was heated for 1 h at 105 °C with the sample mass being monitored and measured during the heating [25]. The %MC was calculated using:

$$\%MC = \frac{mass\ loss}{initial\ mass\ of\ sample} \times 100 \quad (2)$$

The ash content was obtained by completely combusting 1 g of the carbon sample at 750 °C and calculating the percentage ash content using:

$$\%AsC = \frac{mass\ of\ residue}{initial\ mass\ of\ sample} \times 100 \quad (3)$$

Similarly, the volatile mass content was obtained by sample heating in a furnace at 950 °C for 7 mins in the absence of air and the percentage volatile matter content calculated using:

$$\%VM = \frac{weight\ loss}{initial\ weight\ of\ sample} \times 100 \quad (4)$$

The fixed carbon content (FCC) was then calculated as:

$$FCC\ (\%) = 100 - (\%MC + \%AsC\ + \%VM) \quad (5)$$

The Yield was calculated using the mass of the raw precursor material (m_r) and the final activated carbon product (m_P) after carbonization by the following relation:

$$\%Yield = \frac{m_p}{m_r} \times 100\ \% \quad (6)$$

2.2. Electrochemical testing

Initial electrochemical test was done to streamline the amount of samples to be analysed in detail since the main goal was to adopt these materials as energy storage device electrodes.

The three electrode electrochemical analysis were carried out using a Biologic VMP-300 potentiostat (Knoxville, USA) interfaced to a computer using an EC-Lab® V11.02 software. The active sample in form of a slurry was prepared by mixing 85 wt. % of each of the activated carbon samples, 5 wt. % of acetylene black, 10 wt. % polyvinylidene fluoride (PVdF) binder and a few drops of 1-methyl-2-pyrrolidinone (NMP) in an agate mortar. This was coated onto nickel foam (NF) current collectors and dried at 70 °C in an electric oven for 12 h to ensure complete evaporation of the NMP. The mass of actual active material present on the substrate was calculated by subtracting the initial mass of the bare NF from the final mass after coating and drying.

The half-cell (single electrode) charge storage capability (specific capacitance) of each of the as-synthesized activated carbon materials (denoted as AC-M-N) was calculated from the chronopotentiometry (CP) test. To perform analysis in the three electrode set-up, a Ag/AgCl (in saturated KCl) served as the reference electrode (RE) and a glassy carbon plate served as the counter electrode (CE).

The specific capacitance (C_S) was calculated from the slope of the discharge curve of the CP plot by the relation [26].

$$C_{\mathrm{s}}\ (\mathrm{F\ g^{-1}}) = \frac{I * t}{m * \Delta \mathrm{V}} \quad (1)$$

where m is the mass of the active material (in grams), *I* is the current applied (in Amperes), t is the discharge time (in seconds), and ΔV is the potential range (in Volts).

In order to determine the electrochemical performance of a full device, a coin cell system was aseembled for the two electrode tests with each activated sample serving as the electrode separated by a microfiber glass filter paper serving as the separator between the electrodes in a 3.5 M KNO_3 neutral electrolyte.. The filter paper prevents electrical short circuit but allows the movement of ions across the boundary. Detailed studies which included cyclic voltammetry (CV), chronopotentiometry (CP), electrochemical impedance spectroscopy (EIS) and voltage holding (VH) floating test were performed.

2.3. Morphological and Structural characterization

The morphological studies on all samples was carried out using a Zeiss Ultra Plus 55 field emission scanning electron microscope (FE-SEM) operated at 2.0 kV accelerating voltage. Energy dispersive x-ray (EDX) spectroscopy was also done using an accelerating voltage of 20 kV.

Brunauer-Emmett-Teller (BET) method was used to determine the textural properties using a Micromeritics TriStar II 3020 (version 2.00) system at -196 °C in a relative pressure (P/P_o) range of 0.01 – 1.0 for samples pre-degassed at 130 ^{o}C at 500 mTorr (~ 0.8 mbar) for 24 h. The pore size distribution (PSD) was obtained from the desorption branch of the isotherm using the Barrett-Joyner-Halenda (BJH) method.

Raman spectra were collected from the best samples using a Jobin–Yvon Horiba TX 6400 micro-Raman spectrometer with a 532 nm excitation laser which was set at a power of 5 mW.

The system is coupled with a triple monochromator system used for reducing Rayleigh scattering contributions.

Thermogravimetric analysis (TGA) was also carried out on the samples to ascertain their thermal stability. A TGA analyzer (Hitachi STA7300, Japan) was used to monitor the weight variation over increasing temperature in nitrogen atmosphere and subsequently oxygen at the maximum temperature. The samples were heated from room temperature to 1000 °C with a 10 °C min^{-1} ramping rate. At 1000 °C, oxygen was introduced into the chamber to completely burn out the sample.

3. RESULTS AND DISCUSSION

3.1. Single-electrode electrochemical performance, Proximate and Yield Analysis

Table 1 presents a summary of the three electrode tests performed for a single electrode with the specific capacitance and equivalent series resistance (R_S) values for the various carbon-containing raw (AC-CO, AC-PC, AC-RH) materials carbonized with different times. From these results, it was observed that the carbonization time had an influence on the electrochemical behavior of the sample. Although, there was no clear-cut trend observed to all three different samples. Each sample has a unique combination of activating and carbonization requirements to produce an optimized property suitable for energy storage.

The AC-CO sample for example, showed a continuous improvement even as the carbonization times increased. This was not the case with the pine cone (AC-PC) and rice husk (AC-RH) sample as further increasing the time led to a decrease in its storage capability. The observed drop in the C_s value for the pine cone is attributed to a breakdown in the pore structure of

the AC material with longer exposure of the raw material precursor to the carbonization product gas (CO and CO_2) necessary for pore creation at high temperature.

As such, it is proposed that each specific activated carbon material has an optimum carbonization time for a fixed temperature which produces the required hierarchical pore architecture required for efficient ion transport and charge storage. Although the coconut-based AC material showed improvement up to 3 h, it is likely that further exposure times for longer periods at 800 °C will lead to a saturation point. Thereafter, a breakdown of its pore structure in the AC-CO material may be attained and this will eventually affect its storage capability.

From another perspective, using the Table S1 associated with Fig. 2, it is observed that the presence of a higher pore volume consisting of mesopores and micropores also enhanced the charge storage ability which is linked to the recorded specific capacitance value. The samples all showed a relatively good electrochemical behavior in terms of the calculated $C_s$values which ranged between 115 – 300 F g^{-1} at 1 A g^{-1}.

The best samples from the initial electrochemical tests were then selected for detailed material characterization and coupled into a mixed-assembly (asymmetric configuration) two electrode device type for full testing.

In terms of proximate and yield analyses, the selected biomass-sourced activated carbons provided various fixed carbon content depending on the moisture content, ash content and volatile matter content present in each precursor raw material. The results from the proximate analysis and yield values is reported for these selected materials although the values obtained for other samples with different carbonization time was not significantly different for the selected samples. The coconut shell, pine cone and rice husk had a fixed carbon content of ~17.8wt%, ~8.5 wt% and ~12.4wt% respectively. This is comparable to

earlier studies [27, 28] reported on activated carbon from similar biomass raw materials. A detailed summary of the entire proximate analysis and yield for the selected samples is shown in Table 2.

3.2. Morphological and Structural characterization

The SEM images of the best activated carbon samples based on the electrochemical performance from all the three carbon-containing raw material precursors are indicated in Fig. 1 at low and high magnification with the associated EDX pattern. A clear demonstration of a porous structure is seen in all samples after carbonization which is required for active ion transport leading to efficient charge storage (see Fig. S1 of supporting information).

With regards to the EDX profile, the selected samples depicted a high carbon content in the final product with traces of other elements present due to the biological nature of the starting raw material. The AC-PC and AC-RH samples had more quantity of trace elements linked to the biological nature of the raw material precursors as compared to the AC from waste coconut shell. This also could be the reason why the AC-CO electrode recorded the highest half-cell specific capacitance value as compared to the AC-PC and AC-RH electrodes (see table 1). It could be that presence of impurities could also limit the charge storage ability.

On the other hand, a higher number of pores is evident in the AC-PC and AC-CO sample (Fig. 1a-1e) which is confirmed by the BET surface area results reported in Figure 2 and Table S1. From the N_2-adsorption/desorption isotherms, a corresponding BET SSA of 544.1 $m^2\ g^{-1}$ and 584.2 $m^2\ g^{-1}$ was obtained for the AC-CO and AC-PC samples. A much lower BET SSA was obtained for the AC-RH sample. This is further elucidated from the pore size distribution (PSD) plot in Fig. 2b of which the presence of a much higher amount of mesopores and some

micropores was recorded. There is little evidence of significant micropores in the AC-RH sample which explains why it has a much lesser BET SSA and probably a lower *C*s value as compared to the AC-PC and AC-CO samples (see Table 1). The presence of micropores and mesopores within a sample is necessary for charge transport and storage which leads to much better electrochemical performance. Furthermore, the size of these pores are crucial in accommodating specific K^+ ions from the electrolyte which are known to have a crystal and hydration radius suitable for efficient charge transport and storage [29].

Raman analysis is known to be an efficient tool for structurally characterizing carbon materials due to the Raman active nature of carbon materials to laser. The Raman spectra for all three samples were seen to be comparable with the signatory broad D- and G-peaks centered at a wavenumber of 1360 cm^{-1} and 1590 cm^{-1} respectively (see Fig. 3). This confirms a high structurally disordered 3D carbon material created from the biomass raw materials [30–32].

Figure S2 displays the TGA curve coupled with the derivative of the TGA curve associated with all the as-carbonized carbon samples. From the TGA profile for the AC-CO-1 sample shown in Fig. S2(a), a preliminary drop of about 1.28 g is observed at about 86.1 °C which is linked to the loss of moisture within the sample. No other highly significant weight loss is seen in the entire temperature range up to 1000 °C signifying the relative thermal stability of the transformed carbon samples. The indicated weight loss observed from 86.1 °C to 1000 °C is likely related to other species present from the plant origin.

A substantial amount of the carbon material (up to 10.2 mg) is still recorded at the maximum temperature. A further exposure of oxygen to burn out the samples was introduced which burns out the carbon completely as indicated in the DTA plot.

A similar pattern of trend in weight loss was recorded for all samples irrespective of the biomass waste source as well as the carbonization time (see Fig. S2(b-c)). Thus the TGA results revealed no effect of carbonization time on the nature of the thermal stability of the ACs.

3.3. Mixed-Assembly device characterization

Figure 4a and 4b displays the cyclic voltammetry tests results for the mixed-assembly device initially at 20 mV s^{-1}. The initial CV plot (Fig. 4a) is plotted for the current response as a function of operating voltage while Fig. 4b compares the associated C_s with the operating voltage.

In both cases, the PC_RH and RH_CO devices showed the best EDLC behaviour. Although, AC-CO and AC-PC had the highest SSA values as well as highest C_s values, the combination of the activated carbons in a full device leads to a much distinct result.

Interestingly, the mixed assembly containing the AC-CO and AC-PC activated carbon yielded the least current response/specific capacitance. The detailed CV test at different scan rate was then undertaken for the PC_RH device as shown in Fig. 4c. The device retained its ideal EDLC behaviour even as the scan rate was increased up to 100 mV s^{-1}. This shows that the device exhibits a good rate capability required for efficient power delivery [33].

Figures 5a and 5b show the corresponding chronopotentiometry plots at different current densities of 0.5 A g^{-1} and 1.0 A g^{-1} respectively for the three different AC materials. All devices depicted a linear charge/discharge profile which is symmetrically triangular in shape confirming the presence of an EDLC type behaviour with reversible ion-adsorption/desorption on the electrode surface. As observed in the CV plots, the discharge times for both the RH_CO and PC_RH devices are also comparable. By doubling the current density from 0.5 to 1.0 A g^{-}

[1], the specific capacitance becomes more or less the same for both devices. The detailed CP plot of the PC_RH mixed assembly device at increasing current densities is also done and shown in Fig. 5c. The corresponding calculated C_s at each of these current density is reported in Fig. 5d. As current density rises, the discharge time decreases and this is attributed to the inability of the ions to properly access inner pore sites due to the limited ion movement as a result of higher current densities [34, 35].

The Nyquist plot (Fig. 5e) of all mixed-assembly devices relates the unique behaviour of porous carbon-based materials and their electrochemical response at changing frequencies. The PC_RH device once again depicted the typical EDLC behaviour with a relatively short Warburg region as shown in the inset to the Fig. 5e and an almost vertical line at higher frequencies as compared to the other devices. In the high-frequency region, the plot has an intercept value with the real impedance (Z') axis which corresponds to the equivalent series resistance (ESR) value also referred to as the R_S value. This comprises of the resistance of the electrode material, contact resistance at the active material/current collector interface, the internal resistance of the electrode and the electrolyte resistance. A semi-circular arc in the mid-to-high frequency region corresponds to the charge transfer resistance (R_{CT}) which is linked to long-range diffusion and transport channels within the electrode material [33]. Figure 5f depicts the Nyquist plot fitted to a Randles circuit by applying the complex non-linear least-squares technique [36].

A perfectly fitted curve is modelled with the experimental data with the fitting parameters displayed in Table 3. An equivalent series resistance (denoted as R_s) is fitted in series with a constant phase element, CPE (denoted as Q1) needed for the ideal capacitance.

This CPE is also modelled in parallel to the charge transfer resistance (R_{CT}) which is related to the semi-circular arc of the Nyquist plot. The constant phase element Q impedance, is given as:

$$Q = 1/T(j\omega)^n \quad (7)$$

where T is the frequency independent constant with dimensions of (F cm^{-2})^n related to the roughness of the electrode. The *n*-value ranges from -1 to 1 and can be calculated from the gradient of the log Z versus log f plot. When the value of *n* = 0, Q acts as a pure resistor while Q acts as a pure capacitor for n = 1, and acts as an inductor if n = -1 [37].

The Warburg element in the mid-to-high frequency region can be expressed as:

$$W = A/j\omega^n \quad (8)$$

where A is the Warburg coefficient, ω is the angular frequency and n is an exponent [38, 39]. The deviation of the Nyquist plot in the low frequency region from an ideal behaviour of being vertical parallel to the –Z"-axis is attributed to some capacitance leakage (denoted as Q_2). This is also associated with a corresponding leakage resistance (R_2) which is in parallel with Q_2.

In order to further characterize the device for practical application, the stability under pre-set conditions is required. As such, the PC_RH device was subjected to continuous cycling for 10000 continuous charge –discharge cycles at a constant current density. After which the device was further subjected to a voltage holding period of 48 h (2 days). The results from these stability tests are reported in Fig. 6a – 6d. As observed from the plot of the device coulombic efficiency versus cycle number, a drop in efficiency of only 0.3% was observed to retain a final coulombic efficiency of 99.7%. Likewise, the capacitance retention was also calculated at random points during the cyclic tests.

A final capacitance retention of about 80% of its initial capacitance value was observed after 10000 cycles (see Fig. 6b). This shows a good stability of the device under test. In order to ascertain the electrochemical status of the device, the (EIS) test was undertaken once again after cycling and the results are shown in Fig. 6c. The continuous cycling led to no degradation in the capacitive response based on the nature of the Nyquist plot as seen in Fig. 6c. Figure 6d shows the results of the specific capacitance versus voltage holding time at an optimum holding voltage of 1.5 V. The device was observed to be stable at ~80 F g^{-1} for the first 30 h but began to drop in capacitance to a final value of ~53 F g^{-1} which is still more than 50% of its capacitance value.

The Ragone plot showcasing the variation of energy density with power density for the PC_RH device shows a reasonable energy density of 8.5 Wh kg^{-1} and an equivalent power density of 373 W kg^{-1} at 0.5 A g^{-1}. These values are comparable with those reported so far in the literature for such biomass materials and in this case shows a promising step in achieving higher electrochemical performance values based on the mixed-assembly concept.

Thus with proper design and optimization of the synthesis and testing conditions of other activated carbon materials from waste materials, there seems to be a general improvement of the device properties by the incorporation of these materials into a mixed-assembly. This will aid in fully capturing the individual properties of the various materials to obtain a hybrid device.

4. CONCLUSION

In summary, transforming carbon-containing biomass raw waste materials into useful activated carbon for electrochemical capacitors (ECs) has been carried out in this work. The activated carbon nanostructured materials (AC-CO, AC-PC and AC-RH) obtained from these

plant biomass waste materials (coconut shells, pine cones and rice husk) were characterized electrochemically, morphologically, texturally and structurally. The morphological and textural results depict a porous activated carbon materials with necessary pore sites for charge storage obtained from the activation and carbonization process. Devices fabricated from these low cost porous carbons were tested in a mixed assembly type cell (as CO_PC, CO_RH and PC_RH) to maximally capture the individual properties of each of the activated carbons. The results obtained showed that the adoption of such design has its merits and is not solely linked to the individual properties of the materials but the combined functionality in a full device. Although higher specific capacitance values were recorded for the AC-CO and AC-PC samples as compared to the AC-RH. The PC_RH device exhibited the best EDLC properties based on the textural, morphological and structural properties which collectively determines the electrochemical response and extensive stability of the mixed assembly device.

A C_s of 110 F g^{-1}, energy density of 8.5 Wh kg^{-1} and power density of 373 W kg^{-1} was recorded at 0.5 A g^{-1}. A very little loss in coulombic efficiency was observed with the final value remaining at 99.7% and a capacitance retention of up to 80% of its initial value. The voltage holding test showed the device to keep working without failure even after 2 days of subjecting it to an extreme working voltage value. These results are indeed interesting and comparable with and somewhat better than those earlier reported in literature on similar biomass sources [40–42]. The study also provides the pathway in adopting such device configurations for developing efficient and stable electrochemical double layer capacitor devices.

ACKNOWLEDGEMENT

This work is based on the research supported by the South African Research Chairs Initiative of the Department of Science and Technology, Republic of South Africa, National Research Foundation of South Africa (Grant no. 61056) and the African Capacity Building Foundation (ACBF) in conjunction with the Pan African Materials Institute (PAMI) at the African University of Science and Technology, Abuja. Any opinion, finding, conclusion or recommendation expressed in this material is solely that of the author(s). D. Momodu and C. Okafor will like to acknowledge financial support for research from the National Research Foundation (NRF), the University of Pretoria and the African University of Science and Technology (AUST), Abuja.

The authors will also specially like to acknowledge Dr. Farshad Barzegar and Mr Gerald Puts for timely assistance with characterization equipment.

REFERENCES

1. Simon, P., Gogotsi, Y.: Materials for electrochemical capacitors. Nat. Mater. 7, 845–854 (2008).

2. Wang, Y., Song, Y., Xia, Y.: Electrochemical capacitors: mechanism, materials, systems, characterization and applications. Chem. Soc. Rev. 45, 5925–5950 (2016).

3. Béguin, F., Presser, V., Balducci, A., Frackowiak, E.: Carbons and electrolytes for advanced supercapacitors. Adv. Mater. 26, 2219–51, 2283 (2014).

4. Conway, B.E., Birss, V., Wojtowicz, J.: The role and utilization of pseudocapacitance for energy storage by supercapacitors. J. Power Sources. 66, 1–14 (1997).

5. An, G.H., Ahn, H.J.: Activated porous carbon nanofibers using Sn segregation for high-performance electrochemical capacitors. Carbon 65, 87–96 (2013).

6. Sar, P., Ghosh, A., Malik, S., Ray, D., Das, B., Saha, B.: Selective heteroaromatic nitrogen base promoted chromium(VI) oxidation of isomeric pentanols in aqueous micellar media at room temperature. J. Ind. Eng. Chem. 42, 53–62 (2016).

7. Long, C., Jiang, L., Wu, X., Jiang, Y., Yang, D., Wang, C., Wei, T., Fan, Z.: Facile synthesis of functionalized porous carbon with three-dimensional interconnected pore structure for high volumetric performance supercapacitors. Carbon 93, 412–420 (2015).

8. An, H.J., Kim, N.R., Song, M.Y., Yun, Y.S., Jin, H.J.: Fallen-leaf-derived microporous pyropolymers for supercapacitors. J. Ind. Eng. Chem. 45, 223–228 (2017).

9. Wang, D., Liu, S., Fang, G., Geng, G., Ma, J.: From Trash to Treasure: Direct

Transformation of Onion Husks into Three-Dimensional Interconnected Porous Carbon Frameworks for High-Performance Supercapacitors in Organic Electrolyte. Electrochim. Acta. 216, 405–411 (2016).

10. Rolence, C., Machunda, R.L., Njau, K.N.: Potential of Agric Wastes Activated Carbons For Water Softening. Eng. Appl. Sci. 3, 199–207 (2014).

11. Lee, H.-M., Kwac, L.-K., An, K.-H., Park, S.-J., Kim, B.-J.: Electrochemical behavior of pitch-based activated carbon fibers for electrochemical capacitors. Energy Convers. Manag. 125, 347–352 (2016).

12. Lee, D.Y., An, G.H., Ahn, H.J.: High-surface-area tofu based activated porous carbon for electrical double-layer capacitors. J. Ind. Eng. Chem. 52, 121–127 (2017).

13. Wei, L., Yushin, G.: Nanostructured activated carbons from natural precursors for electrical double layer capacitors. Nano Energy. 1, 552–565 (2012).

14. Kalyani, P., Anitha, A.: Biomass carbon & its prospects in electrochemical energy systems. Int. J. Hydrogen Energy. 38, 4034–4045 (2013).

15. Jain, A., Aravindan, V., Jayaraman, S., Kumar, P.S., Balasubramanian, R., Ramakrishna, S., Madhavi, S., Srinivasan, M.P.: Activated carbons derived from coconut shells as high energy density cathode material for Li-ion capacitors. Sci. Rep. 3, 3002 (2013).

16. Divyashree, A., Gurumurthy, H.: Activated carbon nanospheres derived from bio-waste materials for supercapacitor applications – a review. RSC Adv. 5, 88339–88352 (2015).

17. He, X., Ling, P., Yu, M., Wang, X., Zhang, X., Zheng, M.: Rice husk-derived porous carbons with high capacitance by ZnCl2 activation for supercapacitors. Electrochim.

Acta. 105, 635–641 (2013).

18. Ferrero, G.A., Fuertes, A.B., Sevilla, M.: From Soybean residue to advanced supercapacitors. Sci. Rep. 5, 16618 (2015).

19. Bello, A., Manyala, N., Barzegar, F., Khaleed, A.A., Momodu, D.Y., Dangbegnon, J.K.: Renewable pine cone biomass derived carbon materials for supercapacitor application. RSC Adv. 6, 1800–1809 (2016).

20. Farma, R., Deraman, M., Awitdrus, A., Talib, I.A., Taer, E., Basri, N.H., Manjunatha, J.G., Ishak, M.M., Dollah, B.N.M., Hashmi, S.A.: Preparation of highly porous binderless activated carbon electrodes from fibres of oil palm empty fruit bunches for application in supercapacitors. Bioresour. Technol. 132, 254–261 (2013).

21. Abioye, A.M., Noorden, Z.A., Ani, F.N.: Synthesis and Characterizations of Electroless Oil Palm Shell Based-Activated Carbon/Nickel Oxide Nanocomposite Electrodes for Supercapacitor Applications. Electrochim. Acta. 225, 493–502 (2017).

22. Abioye, A.M., Ani, F.N.: Recent development in the production of activated carbon electrodes from agricultural waste biomass for supercapacitors: a review. Renew. Sustain. Energy Rev. 52, 1282–1293 (2015).

23. Xia, H., Meng, Y.S., Yuan, G., Cui, C., Lu, L.: A symmetric carbon / carbon supercapacitor operating at 1 . 6 V by using a neutral aqueous solution. Electrochem. Solid-State Lett. 12, 1275–1278 (2010).

24. Ochai-Ejeh, F.O., Abdulhakeem, B., Dangbegnon, J., Khaleed, A., Madito, M.J., Bazegar, F., Ncholu, M.: High electrochemical performance of hierarchical porous activated carbon derived from lightweight cork (Quercus Suber). J. Mater. Sci. (2017).

25. Department of Forestry, Food and Agrcultural Organization of the United Nations: Report on Quality Control of Charcoal and by-products. http://www.fao.org/docrep/x5555e/x5555e09.htm#TopOfPage (2017).

26. Yang, W., Gao, Z., Wang, J., Ma, J., Zhang, M., Liu, L.: Solvothermal one-step synthesis of Ni-Al layered double hydroxide/carbon nanotube/reduced graphene oxide sheet ternary nanocomposite with ultrahigh capacitance for supercapacitors. ACS Appl. Mater. Interfaces. 5, 5443–5454 (2013).

27. Iqbaldin, M.N.M., Khudzir, I., Azlan, M.I.M., Zaidi, A.G., Surani, B., Zubri, Z.: Properties of coconut shell activated carbon. J. Trop. For. Sci. 25, 497–503 (2013).

28. Dinesh, S.: Development and characterization of pellet activated carbon from new precursors, PhD Dissertation, National Institute of Technology Rourkela, (2011).

29. Barzegar, F., Momodu, D.Y., Fashedemi, O.O., Bello, A., Dangbegnon, J.K., Manyala, N.: Investigation of different aqueous electrolytes on the electrochemical performance of activated carbon-based supercapacitors. RSC Adv. 5, 107482–107487 (2015).

30. Zou, C., Wu, D., Li, M., Zeng, Q., Xu, F., Huang, Z., Fu, R.: Template-free fabrication of hierarchical porous carbon by constructing carbonyl crosslinking bridges between polystyrene chains. J. Mater. Chem. 20, 731 (2010).

31. Yao, L., Yang, G., Han, P., Tang, Z., Yang, J.: Three-dimensional beehive-like hierarchical porous polyacrylonitrile-based carbons as a high performance supercapacitor electrodes. J. Power Sources. 315, 209–217 (2016).

32. Mao, Y., Duan, H., Xu, B., Zhang, L., Hu, Y., Zhao, C., Wang, Z., Chen, L., Yang, Y.:

Lithium storage in nitrogen-rich mesoporous carbon materials. Energy Environ. Sci. 5, 7950 (2012).

33. Bello, A., Barzegar, F., Momodu, D., Dangbegnon, J., Taghizadeh, F., Manyala, N.: Symmetric supercapacitors based on porous 3D interconnected carbon framework. Electrochim. Acta. 151, 386–392 (2015).

34. Reddy, R.N., Reddy, R.G.: Porous structured vanadium oxide electrode material for electrochemical capacitors. J. Power Sources. 156, 700–704 (2006).

35. Lao, Z.J., Konstantinov, K., Tournaire, Y., Ng, S.H., Wang, G.X., Liu, H.K.: Synthesis of vanadium pentoxide powders with enhanced surface-area for electrochemical capacitors. J. Power Sources. 162, 1451–1454 (2006).

36. Randles, J.E.B.: Kinetics of rapid electrode reactions. Discuss. Faraday Soc. 1, 11 (1947).

37. Guan, H., Fan, L.-Z., Zhang, H., Qu, X.: Polyaniline nanofibers obtained by interfacial polymerization for high-rate supercapacitors. Electrochim. Acta. 56, 964–968 (2010).

38. Zhou, Y., Xu, H., Lachman, N., Ghaffari, M., Wu, S., Liu, Y., Ugur, A., Gleason, K.K., Wardle, B.L., Zhang, Q.M.: Advanced asymmetric supercapacitor based on conducting polymer and aligned carbon nanotubes with controlled nanomorphology. Nano Energy. 9, 176–185 (2014).

39. Masarapu, C., Zeng, H.F., Hung, K.H., Wei, B.: Effect of temperature on the capacitance of carbon nanotube supercapacitors. ACS Nano. 3, 2199–2206 (2009).

40. Ma, G., Li, J., Sun, K., Peng, H., Feng, E., Lei, Z.: Tea-leaves based nitrogen-doped porous carbons for high-performance supercapacitors electrode. J. Solid State

Electrochem. doi: 10.1007/s10008-016-3389-y (2016).

41. Chen, X., Wu, K., Gao, B., Xiao, Q., Kong, J., Xiong, Q., Peng, X., Zhang, X., Fu, J.: Three-Dimensional Activated Carbon Recycled from Rotten Potatoes for High-performance Supercapacitors. Waste and Biomass Valorization. 7, 551–557 (2016).

42. Luo, Q.-P., Huang, L., Gao, X., Cheng, Y., Yao, B., Hu, Z., Wan, J., Xiao, X., Zhou, J.: Activated carbon derived from melaleuca barks for outstanding high-rate supercapacitors. Nanotechnology. 26, 304004 (2015).

LIST OF FIGURES

Figure 1: SEM image at low and higher magnification accompanied with related EDX spectra for activated carbon from (a-c) coconut; (d-f) pine cone and (g-i) rice husk

Figure 2: (a) N_2 absorption/desorption isotherm; (b) pore size distribution for the different activated samples from various carbon precursors

Figure 3: (a) Raman analysis of the different activated samples from various carbon precursors

Figure 4: (a, b) CV plot of full mixed-assembly device composed of different carbon precursors showing variation of current response and specific capacitance with voltage at 20 mV s^{-1}; and (c) detailed CV curves for the PC_RH device at varying scan rates of 10 – 100 mV s^{-1}.

Figure 5: (a,b) Charge-discharge curves of the full device for different carbon precursors at 0.5 and 1.0 A g^{-1} respectively; (c) detailed charge-discharge profile at current densities of 0.5 – 5.0 A g^{-1};(d) variance of specific capacitance (C_s) at different current densities; (e) Nyquist plot of all the ACPR electrodes from different carbon precursors with the figure inset illustrating the equivalent series resistance (ESR) in the high frequency region and (f) EIS plot fitting of PC_RH electrode

Figure 6: (a) Coulombic efficiency versus cycle number(b) Capacitance retention versus cycle number showing the device stability after 10000 cycles at 5 A g^{-1}; (c) Nyquist plot before and after cycling for the mixed-assembly device (d) capacitance retention versus voltage holding time for 48 h; (e) Ragone plot showing the energy density as a function of power density

Table 1: A summary of the 3-electrode electrochemical characterization on the samples obtained with varying carbonization times at 800 °C with a KOH:active raw material ratio of 1:1

Table 2: A summary of the Proximate and Yield analysis done for the various carbon precursors

Table 3: Calculated values of fitted parameters through CNLS fitting of the experimental impedance spectra based on equivalent circuit shown in the inset to Fig. 5f

Fig. S1. SEM micrographs of samples carbonized from coconut shells, pinecones and rice husk biomass waste for 1, 2 and 3 h carbonization times.

Fig. S2. (a) Detailed TGA analysis with associated DTG plots for AC-CO-1 sample (b-c) summarized results from TGA profile and DTG profile of samples carbonized from coconut shells, pinecones and rice husk biomass waste for 1, 2 and 3 h carbonization times.

Table S1. Table summarizing the textural properties for all activated carbon samples

Graphical Abstract

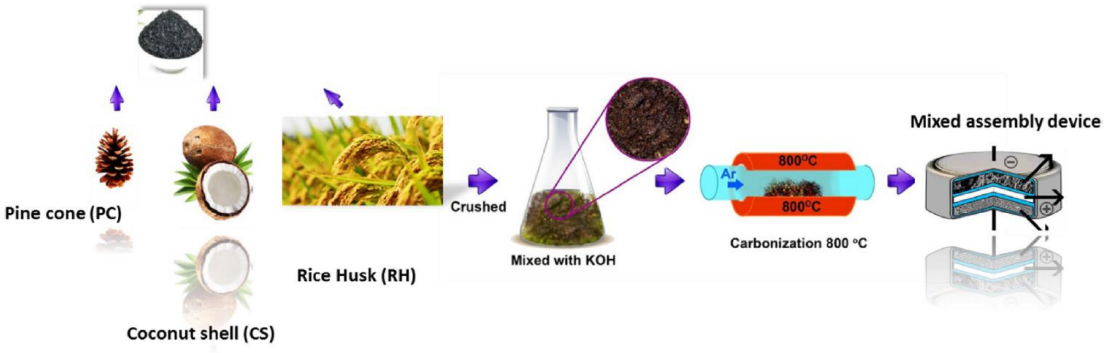

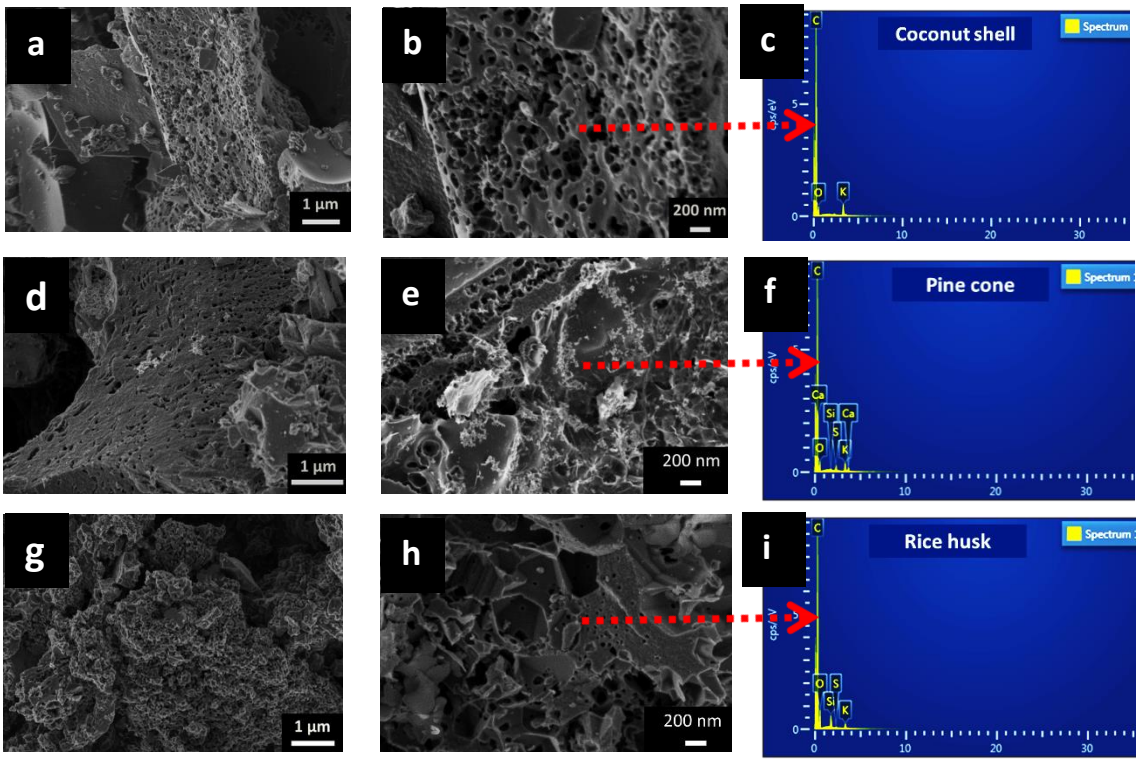

Figure 1: SEM image at low and higher magnification accompanied with related EDX spectra for activated carbon from (a-c) coconut; (d-f) pine cone and (g-i) rice husk

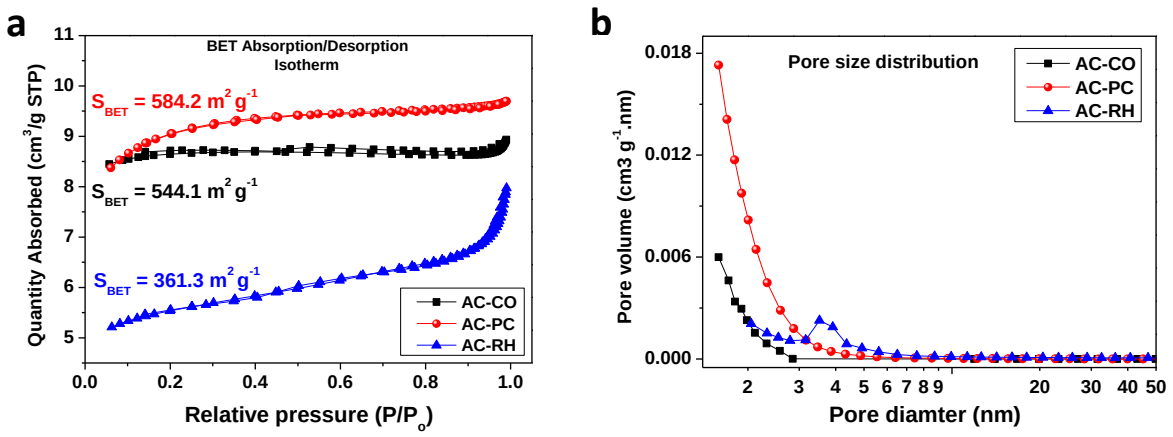

Figure 2:(a) N_2 absorption/desorption isotherm; (b) pore size distribution for the different activated samples from various carbon precursors

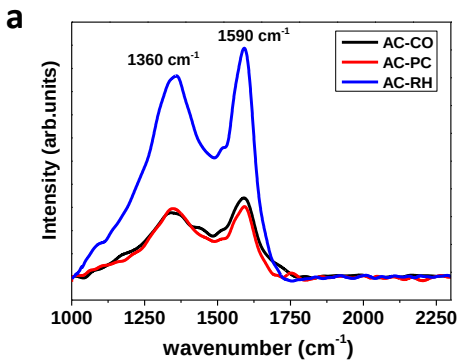

Figure 3: (a) Raman analysis of the different activated samples from various carbon precursors

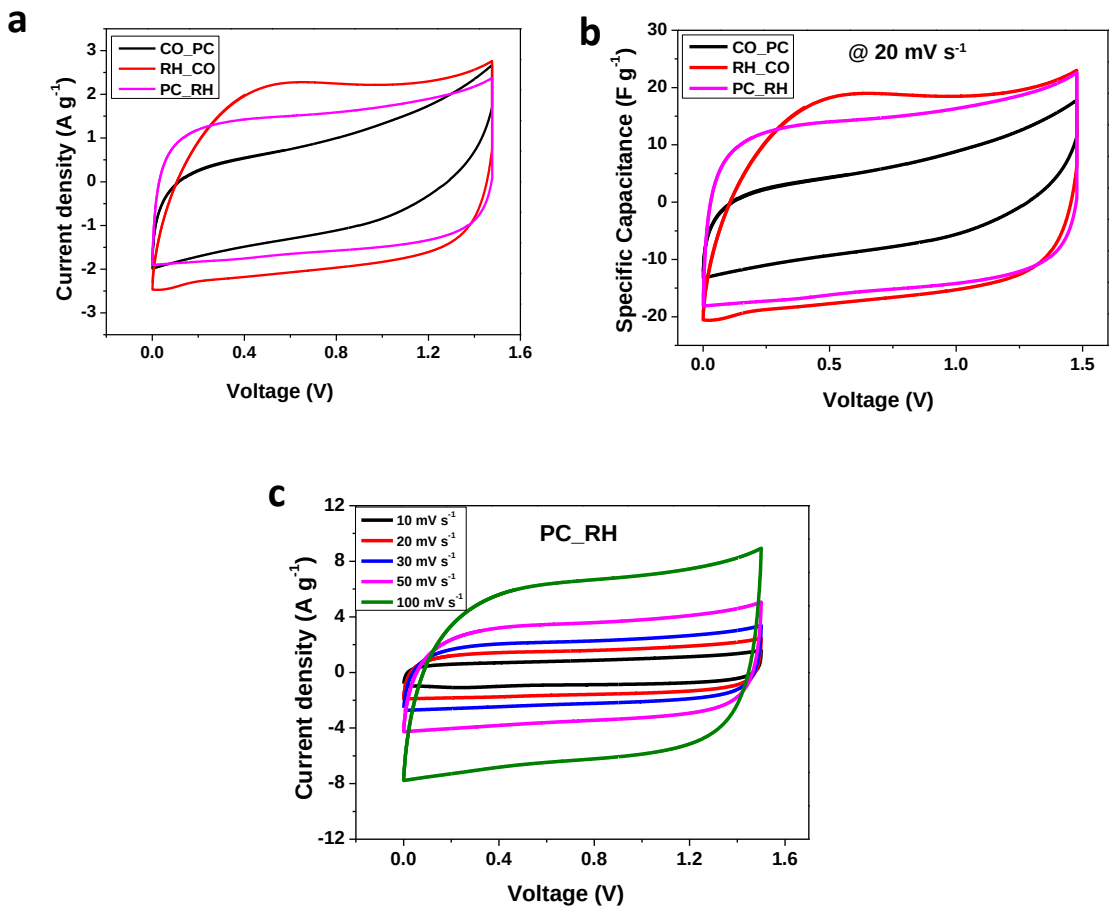

Figure 4: (a, b) CV plot of full mixed-assembly device composed of different carbon precursors showing variation of current response and specific capacitance with voltage at 20 mV s^{-1}; and (c) detailed CV curves for the PC_RH device at varying scan rates of 10 – 100 mV s^{-1}.

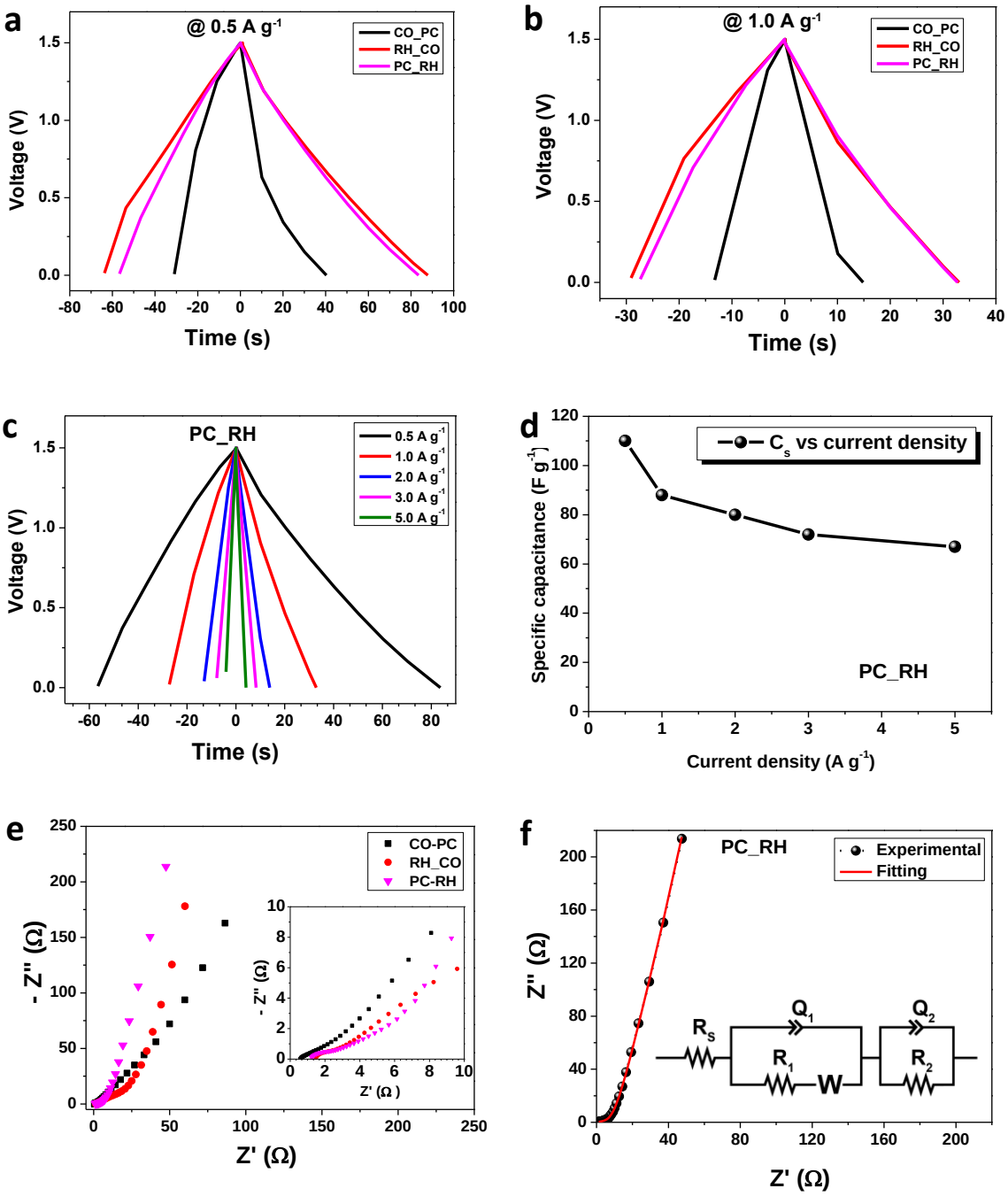

Figure 5: (a,b) Charge-discharge curves of the full device for different carbon precursors at 0.5 and 1.0 A g^{-1} respectively; (c) detailed charge-discharge profile at current densities of 0.5 – 5.0 A g^{-1};(d) variance of specific capacitance (C_s) at different current densities; (e) Nyquist plot of all the ACPR electrodes from different carbon precursors with the figure inset illustrating the equivalent series resistance (ESR) in the high frequency region and (f) EIS plot fitting of PC_RH electrode

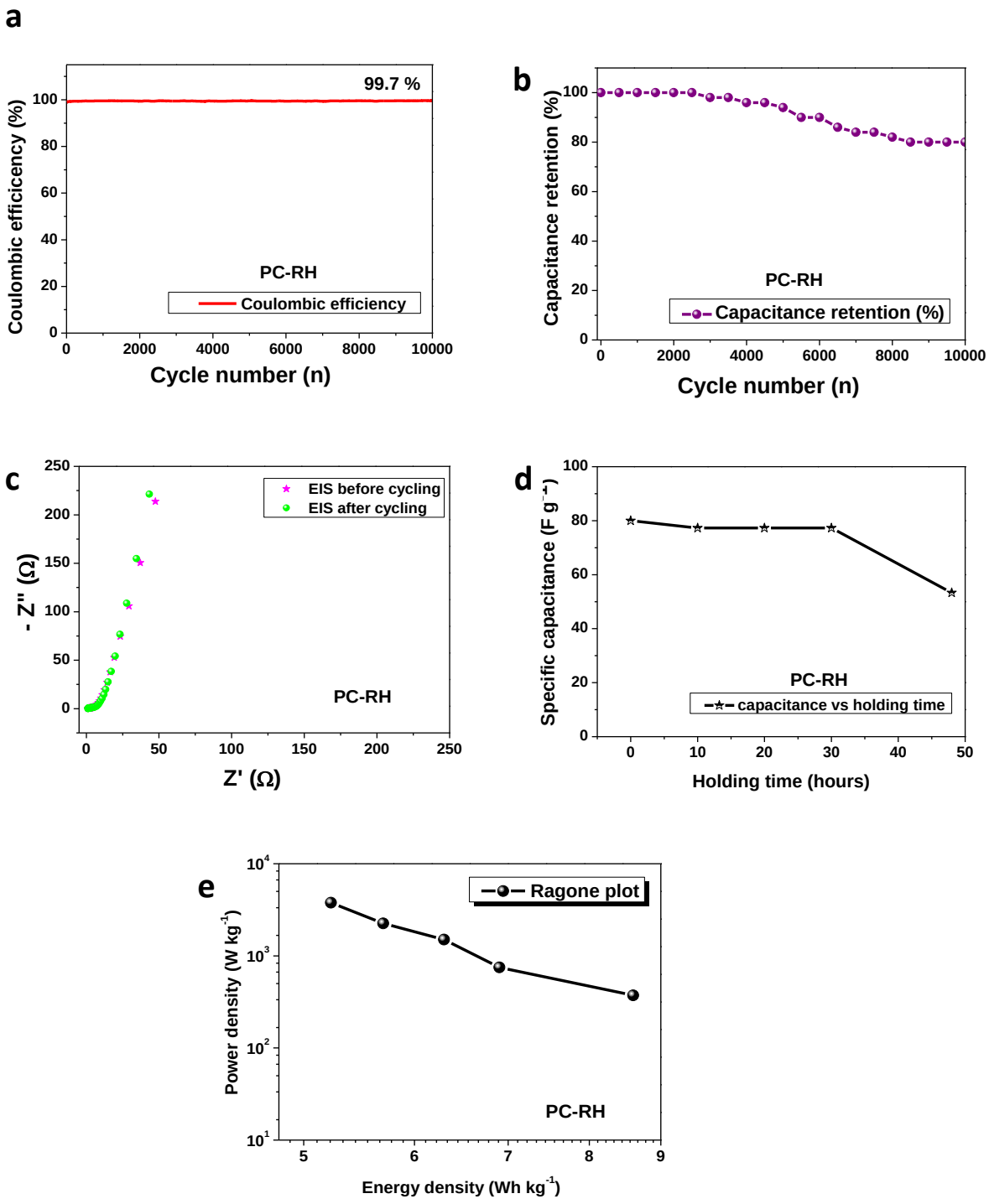

Figure 6: (a) Coulombic efficiency versus cycle number(b) Capacitance retention versus cycle number showing the device stability after 10000 cycles at 5 A g^{-1}; (c) Nyquist plot before and after cycling for the mixed-assembly device (d) capacitance retention versus voltage holding time for 48 h; (e) Ragone plot showing the energy density as a function of power density

Table 1: A summary of the 3-electrode electrochemical characterization on the samples obtained with varying carbonization times at 800 °C with a KOH:active raw material ratio of 1:1

Sample electrode (AC-M-N)	**Specific capacitance** (C_s in F g^{-1})@ 1 A g^{-1}
AC-CO-1	115.00
AC-CO-2	191.67
AC-CO-3	300.00
AC-PC-1	214.29
AC-PC-2	205.71
AC-PC-3	181.43
AC-RH-1	125.00
AC-RH-2	161.17
AC-RH-3	148.33

Table 2: A summary of the Proximate and Yield analysis done for the various carbon precursors

Biomass source	**Moisture content %MC**	**%AC (Ash content)**	**%VM (Volatile matter content)**	**%FC (Fixed carbon content)**	**%Yield**
Coconut shell	**6.5**	**25.3**	**50.4**	**17.8**	**52.37**
Pine cone	**25.6**	**6.1**	**59.8**	**8.5**	**43.08**
Rice husk	**8.2**	**32.4**	**47.0**	**12.4**	**47.56**

Table 3: Calculated values of fitted parameters through CNLS fitting of the experimental impedance spectra based on equivalent circuit shown in the inset to Fig. 5f

Electrode	**R_s(Ω)**	**R_1(Ω)**	**Q_1(F)**	**R_2(Ω)**	**Q_2 ()**
AC-PC-RH	**1.22**	**1.32**	**-**	**-**	**-**
X^2 = 0.02, X/$\sqrt{N}$= -, Q ≡CPE, a≡ n					

SUPPORTING INFORMATION

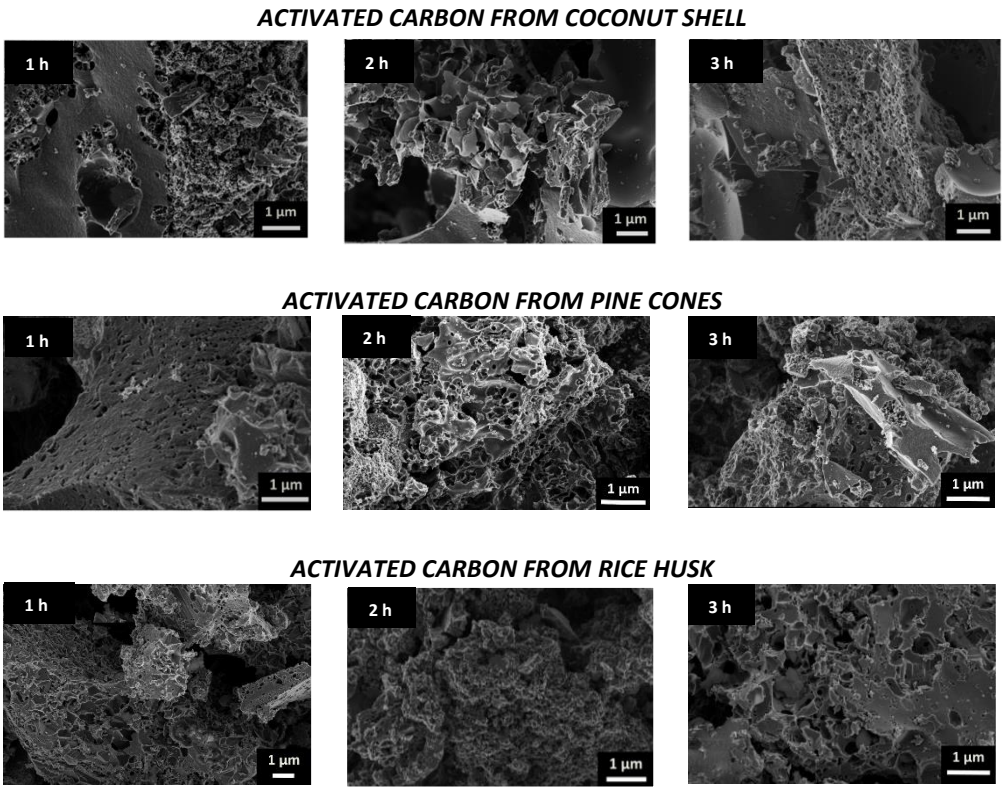

Fig. S1. SEM micrographs of samples carbonized from coconut shells, pinecones and rice husk biomass waste for 1, 2 and 3 h carbonization times.

Table S1. Table summarizing the textural properties for all activated carbon samples

Sample electrode (AC-M-N)	Specific capacitance @ 1 A/g (C_s in F/g)	Specific surface area (SSA in $m^2 g^{-1}$)	Total pore volume[x] (V_{Total}, $cm^3 g^{-1}$)	Micropore volume[y] (V_{micro}, $cm^3 g^{-1}$)
AC-CS-1	115.00	266.95	0.171	0.130
AC-CS-2	191.67	334.44	0.185	0.011
AC-CS-3	300.00	544.05	0.306	0.280
AC-PC-1	214.29	584.15	0.335	0.232
AC-PC-2	205.71	503.68	0.314	0.241
AC-PC-3	181.43	297.02	0.181	0.157
AC-RH-1	125.00	275.93	0.206	0.135
AC-RH-2	161.17	361.39	0.265	0.148
AC-RH-3	148.33	279.08	0.208	0.132

[x]Total pore volume obtained from the N_2 uptake at $P/P_0 = 0.99$. [y]pore volume obtained from t-plot analysis. [z]Mesopore volume ($V_{meso} = V_{Total} - V_{micro}$).

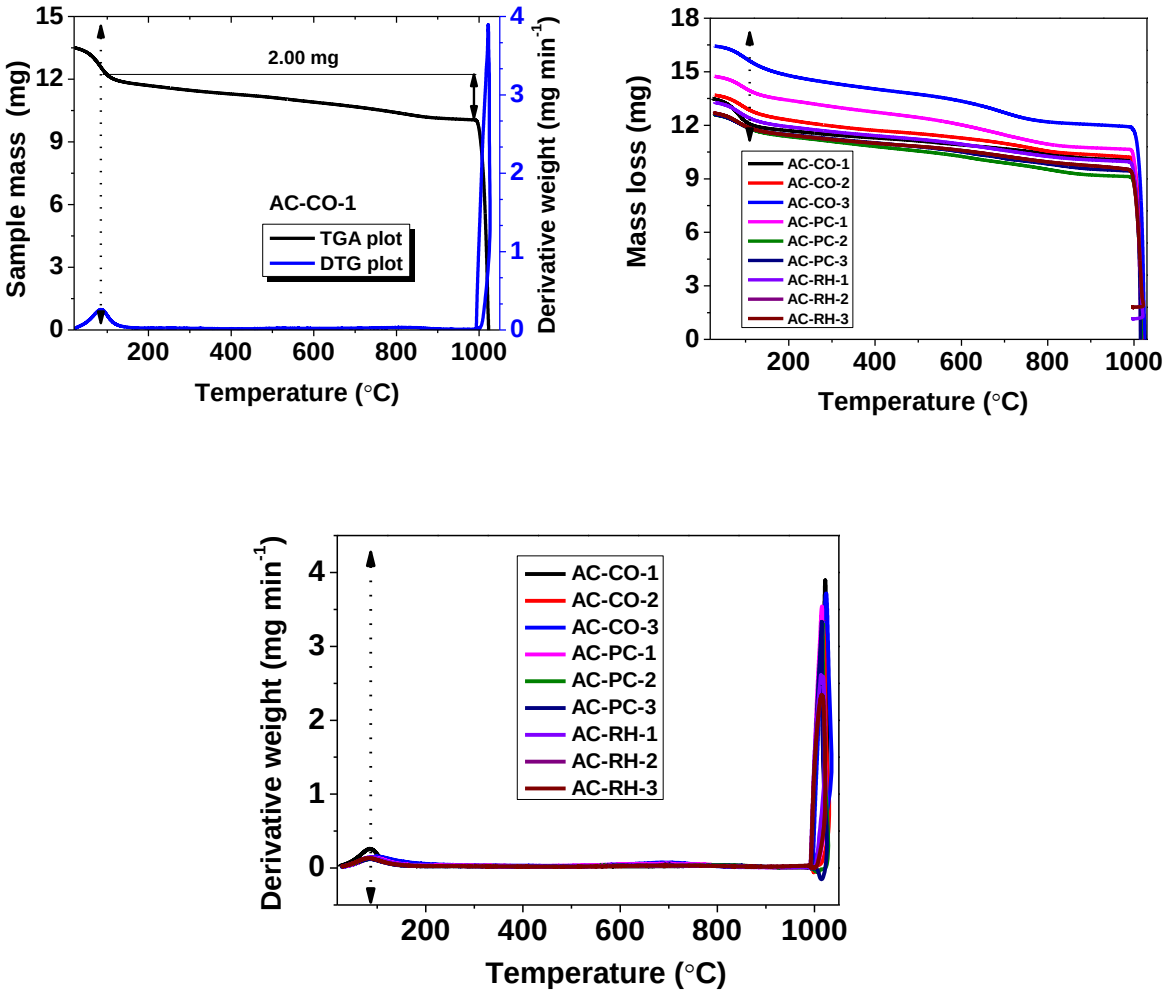

Fig. S2. (a) Detailed TGA analysis with associated DTG plots for AC-CO-1 sample (b-c) summarized results from TGA profile and DTG profile of samples carbonized from coconut shells, pinecones and rice husk biomass waste for 1, 2 and 3 h carbonization times.